JASMAC Conference of the Japan Society of Microgravity Application

OR1-6

DARTS 公開データを使用した FACET 実験のデータ解析

Data Analysis of FACET Experiment by Use of Open Data Stored in Kibo Experiment Data Archive of DARTS

足立 聡
Satoshi ADACHI
宇宙航空研究開発機構，Japan Aerospace Exploration Agency

1. Introduction

FACET experiment was carried out in 2009 and 2010 on orbit [1]. The experimental data are opened and are available on the DARTS (Data Archives and Transmission System) website [2]. The data can be freely used for academic and educational purposes.

The objectives of FACET experiment are to investigate conditions causing faceted morphological instability and to investigate mechanisms of faceted morphological instability. Faceted cellular growth of anisotropic materials is a target phenomenon in the FACET experiment. The similar instability in the isotropic materials is well known as the Mullins-Sekerka morphological instability. However, it is not clarified whether the faceted instability is the same mechanism as the Mullins-Sekerka instability or not.

Thus, a two-wavelength interferometer and an amplitude modulation microscope, which are installed in the Solution Crystallization Observation Facility (SCOF), are used to achieve the objectives. Temperature and concentration distributions are obtained from the interferometer measurements.

There are several issues to fully understand the instability mechanisms, that is, dependency of growth rate on supersaturation to identify the growth mechanisms, microscopic observation to find the beginning location of instability, description of instability model to understand the instability mechanisms. The dependency of growth rate on supersaturation is investigated in this paper as the first step.

2. Experimental Setup

The SCOF is located on the 'Kibo' module of the international space station (ISS). The SCOF has a two-wavelength Mach-Zehnder interferometer and an amplitude modulation microscope. Magnification factors are two and four. The sizes of the field of view are 2.4 mm×3.6 mm and 1.2 mm×1.8 mm, respectively. The SCOF optical observation devices are schematically shown in **Figure 1(a)**. The experiment cell shown in **Figure 1(a)** is schematically shown in **Figure 1(b)**. Mixture of phenyl salicylate (Salol) and *tert*-butyl alcohol (*t*-butanol) is put into the cell and sealed.

Two cells are installed in one cartridge. Initial target concentrations of *t*-butanol are 4 mol% and 8 mol%, respectively. After the experiment, the cartridge is returned on the ground. The *t*-butanol concentrations are measured and is found that those are 1.15 mol% and 2.58 mol%, respectively. The concentration decrease may

be caused by the vaporization of *t*-butanol during the sample preparation. Although the concentration differs from the target concentration, this is not a big problem because the known concentration is the most important to obtain concentration distributions. In this paper, run number 9 (named as FACET2-07) is used as the typical experimental result. The temperature gradient and the cooling rate are 15 K/cm and 2 K/min, respectively.

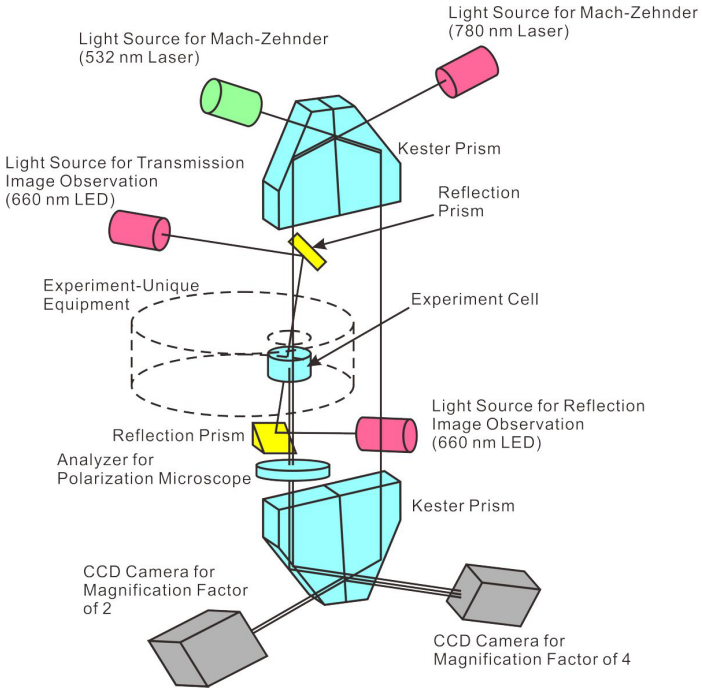

(a) Schematic view of SCOF optical observation devices

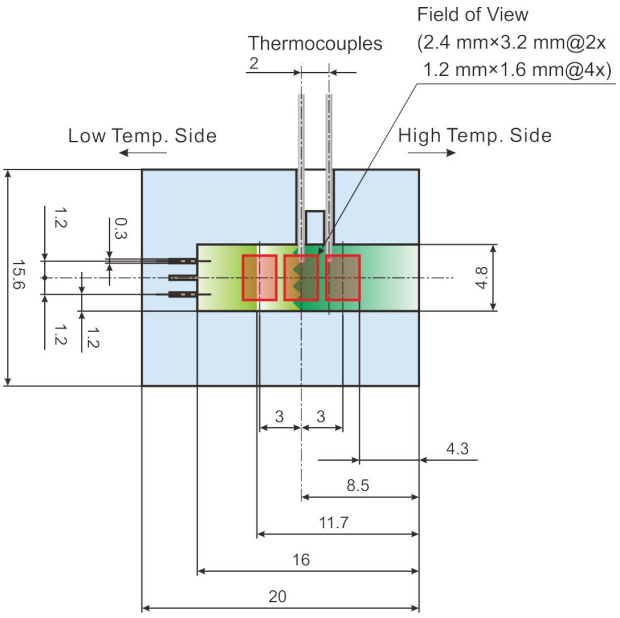

(b) Schematic view of FACET experiment cell

Figure 1. Schematic view of SCOF optical observation devices and FACET experiment cell.

3. Data Analysis Method

The main data are interferometric images. The temperature and concentration distributions are obtained by

analyzing the interferometric images. A two-dimensional Fourier transform is used in this paper to analyze the interferometric image. This method has features of no need of additional images and reasonable calculation time. The temperature and concentration are calculated by using the following equations.

$$T = \frac{\Delta(\Delta\phi)_1 \frac{\lambda_{0_1}}{2\pi L_s} b_2 - \Delta(\Delta\phi)_2 \frac{\lambda_{0_2}}{2\pi L_s} b_1}{\left(a_1 + a_3 \frac{L_g}{L_s}\right) b_2 - \left(a_2 + a_4 \frac{L_g}{L_s}\right) b_1} + T(0) \text{ and} \tag{1}$$

$$C = \frac{\Delta(\Delta\phi)_1 \frac{\lambda_{0_1}}{2\pi L_s}\left(a_2 + a_4 \frac{L_g}{L_s}\right) - \Delta(\Delta\phi)_2 \frac{\lambda_{0_2}}{2\pi L_s}\left(a_1 + a_3 \frac{L_g}{L_s}\right)}{\left(a_2 + a_4 \frac{L_g}{L_s}\right) b_1 - \left(a_1 + a_3 \frac{L_g}{L_s}\right) b_2} + C(0) \tag{2}$$

where $\Delta(\Delta\phi)_1 = \Delta\phi_1(t) - \Delta\phi_1(0)$, $\Delta(\Delta\phi)_2 = \Delta\phi_2(t) - \Delta\phi_2(0)$, L_g, L_s, λ_{0_1}, λ_{0_2}, $\Delta\phi_1$, $\Delta\phi_2$, $T(0)$, and $C(0)$ represent phase change at the wavelength of the first laser (wavelength of 532 nm), phase change at the wavelength of the second laser (wavelength of 780 nm), the thickness of glass cell, sample thickness, wavelength of the first laser in vacuum (532 nm), and wavelength of the second laser in vacuum (780 nm), phase change at the wavelength of the first laser, phase change at the wavelength of the second laser, the temperature at $t = 0$, and the concentration at $t = 0$, respectively. The parameters a_1, a_2, a_3, a_4, b_1, and b_2 are expressed as

$$a_1 = \left(\frac{\partial n_1}{\partial T}\right)_s, a_2 = \left(\frac{\partial n_2}{\partial T}\right)_s, a_3 = \left(\frac{\partial n_1}{\partial T}\right)_g, a_4 = \left(\frac{\partial n_2}{\partial T}\right)_g, b_1 = \left(\frac{\partial n_1}{\partial C}\right)_s, \text{and } b_2 = \left(\frac{\partial n_2}{\partial C}\right)_s, \tag{3}$$

where n_1 and n_2 are refractive indices at the wavelength of the first and second lasers, respectively. Since denominators of **Eqs.** (1) and (2) are subtractions of multiplications, the parameters a_1 to b_2 should have high precision at least four digits of accuracy. This is the reason why the two-wavelength interferometer is not well familiar. Since it is not easy to obtain such precision due to easy vaporization of *t*-butanol, the refractive indices of sample have been measured several times. As a result, the parameters a_1, a_2, b_1, and b_2 are determined as

$$\begin{aligned}
&\left(\frac{\partial n_1}{\partial T}\right)_C = -3.8843 \times 10^{-4} \ [1/\mathrm{K}], \\
&\left(\frac{\partial n_2}{\partial T}\right)_C = -2.3867 \times 10^{-4} \ [1/\mathrm{K}], \\
&\left(\frac{\partial n_1}{\partial C}\right)_T = -6.7583 \times 10^{-4} \ [1/\mathrm{mol\%}], \text{and} \\
&\left(\frac{\partial n_2}{\partial C}\right)_T = -6.3917 \times 10^{-4} \ [1/\mathrm{mol\%}].
\end{aligned} \tag{4}$$

Since temperature dependency of refractive indices of fused quartz has weak dependency on wavelength, a_3 and a_4 are the same value and are expressed as

$$\left(\frac{\partial n_1}{\partial T}\right)_g \simeq \left(\frac{\partial n_2}{\partial T}\right)_g \simeq 8 \times 10^{-6} \ [1/\mathrm{K}]. \tag{5}$$

Thus, **Eqs.** (1) and (2) are calculated.

4. Experimental Results and Discussion

The typical results of stable growth are shown in **Figure 2**. All images are obtained under the condition of

the magnification factor of 2. **Figure 2(a)** is the amplitude modulation microscopic image, **Figure 2(b)** is the interferometric image with the wavelength of 532 nm, and **Figure 2(c)** is the interferometric image with the wavelength of 780 nm. It is found that the fringes are curved near the interface. Since the temperature distribution is much more linear than the concentration distribution, the curved fringe shows the concentration is piled up near the interface due to segregation.

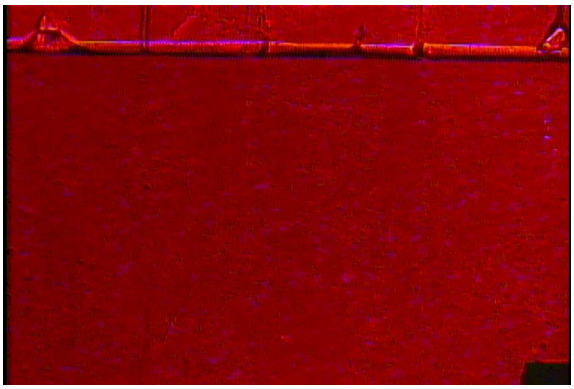

(a) Amplitude modulation microscopic image

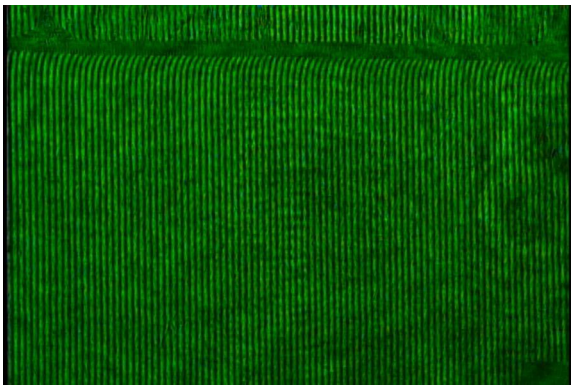

(b) Interferometric image with wavelength of 532 nm

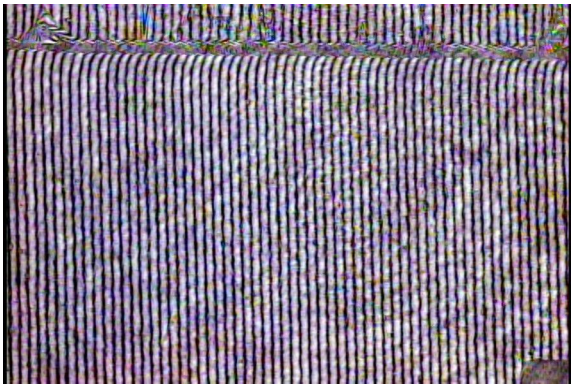

(c) Interferometric image with wavelength of 780 nm

Figure 2. Typical experimental results of stable growth

The phase distribution is calculated from the interferometric images to calculate the temperature and concentration. The noise reduction is required as the first step of calculation. Two-dimensional Fourier transform is executed. There should be some peaks, but the peak positions are unclear due to noises. To reduce the noises, the amplitude is calculated. Amplitude clearly shows the peaks. The peak at the center mainly consists of fringe information. Therefore, the next peak on the right side of the center peak is selected as the signal.

The inverse Fourier transform of this peak is executed. **T**he amplitude of the inverse Fourier transform clearly shows that the fringes are fully eliminated. To obtain phase distribution, the following equation is used.

$$\phi = \tan^{-1}\left\{\frac{Im(I_F)}{Re(I_F)}\right\}. \tag{6}$$

The calculated results of **Eq.** (6) are shown in **Figure 3**. **Figure 3(a)** represents the phase change from $-\pi/2$ to $\pi/2$ at the wavelength of 532 nm. **Figure 3(b)** is an unwrapped phase distribution. It is found that the phase unwrapping is smooth and successful though a few phase singularities exist. **Figure 3(c)** is the phase change

at 780 nm, and **Figure 3(d)** is the unwrapped phase distribution. Thus, **Eqs.** (1) and (2) are calculated by using obtained two phase changes $\Delta\phi_1$ and $\Delta\phi_2$. Since there are no data on refractive indices of the solid phase of phenyl salicylate / *tert*-butanol alloy, phase unwrapping and phase calculation in the liquid phase are correct.

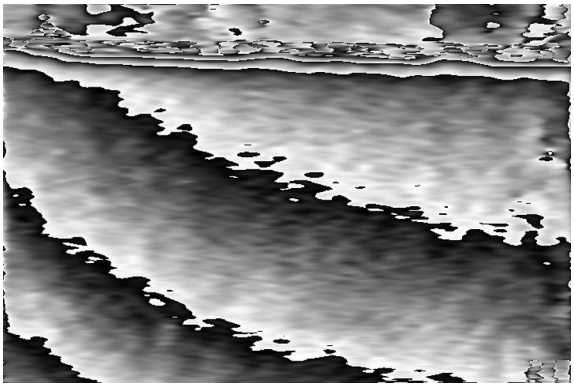

(a) Phase change at 532 nm

(b) Unwrapped phase at 532 nm

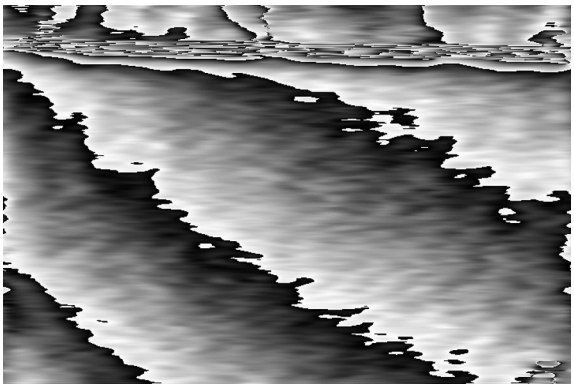

(c) Phase change at 780 nm

(d) Unwrapped phase at 780 nm

Figure 3. Calculated phases at 532 nm and 780 nm

By calculating **Eqs.** (1) and (2), the temperature and concentration distributions in the liquid phase are obtained and are shown in **Figure 4**. **Figure 4(a)**, **Figure 4(b)**, **Figure 4(c)**, and **Figure 4(d)** represent temperature in stable growth, concentration in stable growth, temperature in faceted cellular growth, and concentration in faceted cellular growth, respectively. It is found that the temperature decreases with time advancement and the concentration piles up over time. This behavior seems to be reasonable.

The dependency of growth rate on supersaturation is investigated from the interferometric measurements to investigate not only the growth mechanisms but also measurement accuracy, especially a measurement offset. The dependency is shown in **Figure 5**. Red circles and blue circles represent growth rates at a vertex location of faceted cell and growth rates at a valley location of faceted cell, respectively. It seems that the offset is about 1 % or less. It is found that three kinds of growth mechanisms exist, that is, adhesive growth, spiral growth, and two-dimensional nucleation growth. It is also found that both growth rates at the vertex and at the valley are sit on the same line. This means that the growth mechanisms at the vertex and at the valley are the same.

To confirm this hypothesis, the time evolution of interface movement is investigated and is shown in **Figure 6(a)**. The result clearly shows that the interface movement at the vertex is faster than that at the valley during

the time from 3.6 to 4.7 min, but the interface movement is almost the same after that time. **Figure 6(b)** shows the time evolution of supersaturation. This shows the supersaturation at the vertex is larger than that at the valley from 3.6 to 4.7 min, but the supersaturation at the vertex is almost the same or smaller than that at the valley except for that time. This is the reason why the growth rate at the vertex is similar to that at the valley after 4.7 min. As a conclusion, no special growth mechanism exists at the vertex.

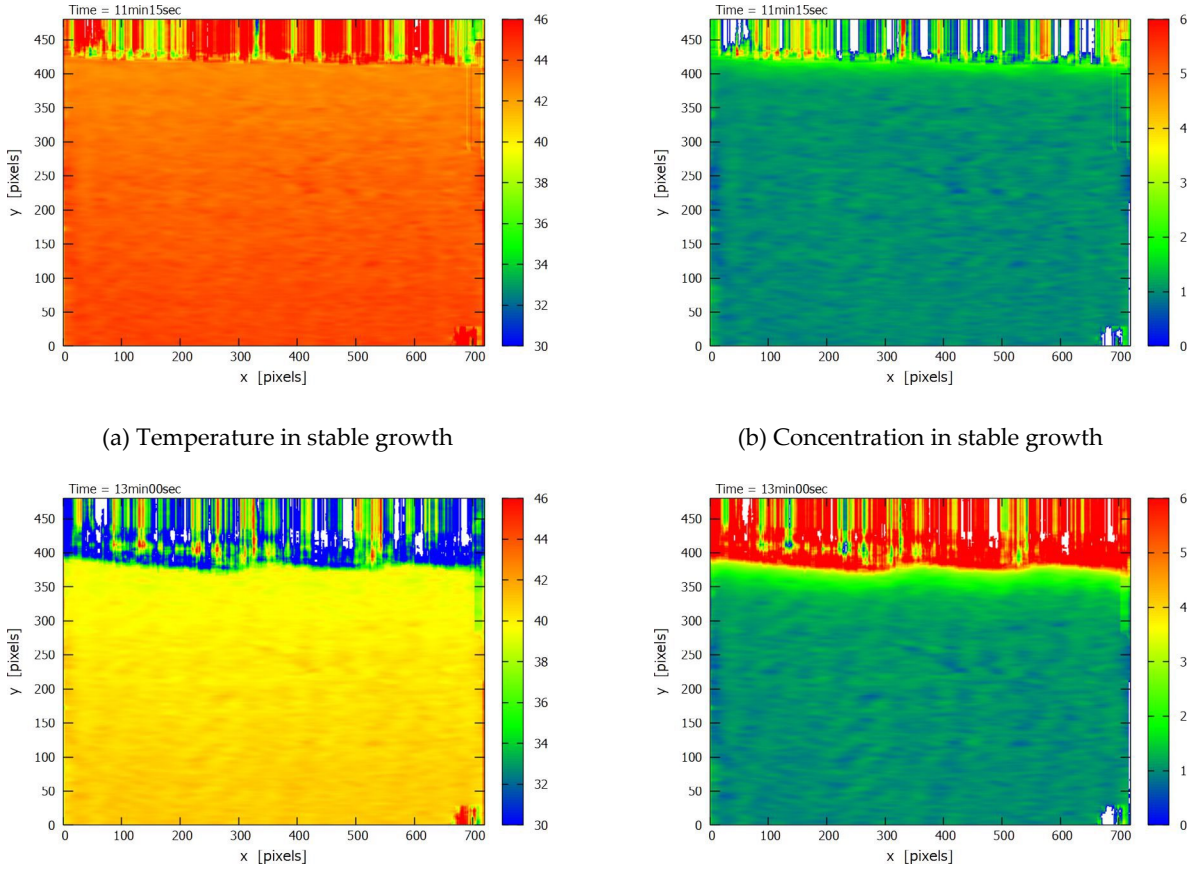

(a) Temperature in stable growth

(b) Concentration in stable growth

(c) Temperature in faceted cellular growth

(d) Concentration in faceted cellular growth

Figure 4. Temperature and concentration distributions in stable growth and in faceted cellular growth

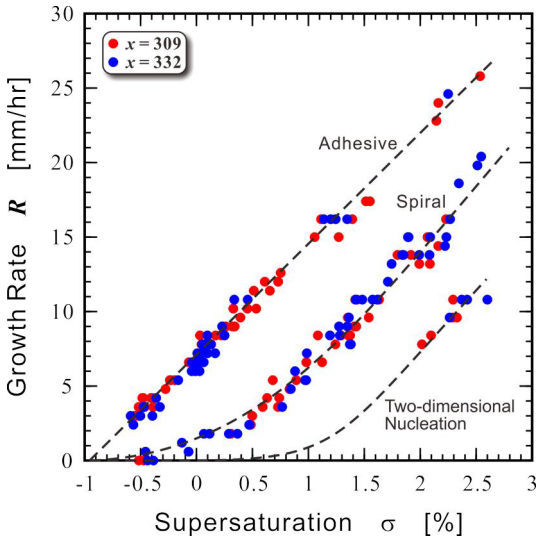

Figure 5. Growth rate dependency on supersaturation

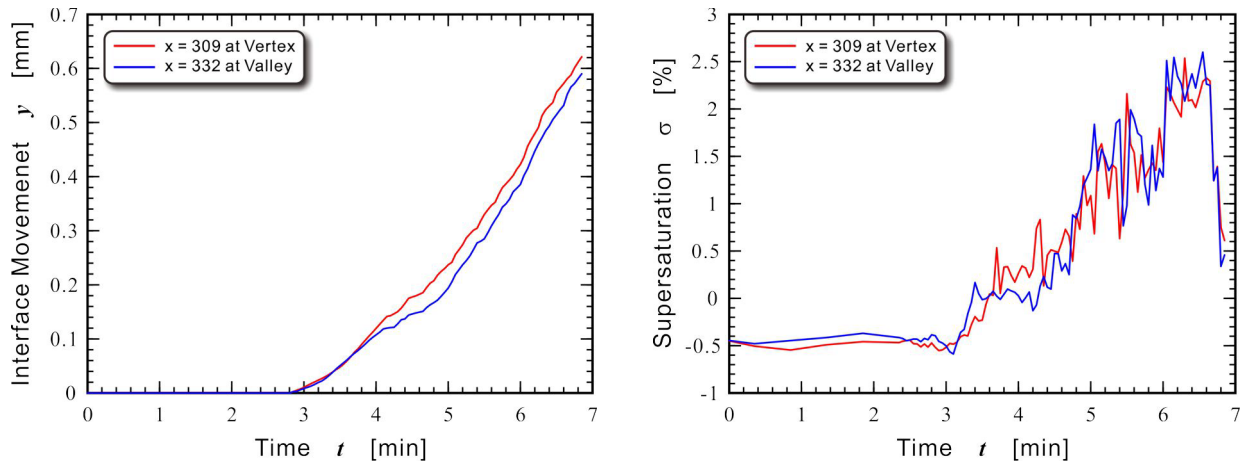

(a) Interface movement (b) Supersaturation

Figure 6. Time evolution of interface movement and supersaturation

5. Conclusions

Data analysis of faceted cellular growth, FACET experiment, is carried out by using the open data being available on the DARTS. The dependency of the growth rate on the supersaturation is investigated to understand the growth mechanisms. The offset of supersaturation may be 1 % or less from the dependency. The dependency shows that there are three mechanisms, that is, adhesive growth, spiral growth, and two-dimensional nuclear growth. No new growth mechanisms exist. This means that the trigger of morphological instability should be the supersaturation variation.

References

1) Y. Inatomi: Rapid Communication: Crystal Growth Experiments in KIBO, J. Jpn. Soc. Microgravity Appl., **27** (2010) 32.
2) https://darts.isas.jaxa.jp/iss/kibo/

Acknowledgements

FACET data are obtained from Kibo Experiment Data Archive, which is a part of DARTS (Data Archives and Transmission System). The author is grateful to all concerned with DARTS for their efforts to open valuable data and to keep opening them.